Revisiting wrong sign Yukawa coupling of type II two-Higgs-doublet model in light of recent LHC data*

Lei Wang(王磊) Hong-Xin Wang(王宏昕) Xiao-Fang Han(韩小芳)[1)]

Department of Physics, Yantai University, Yantai 264005, China

Abstract: In light of the recently obtained LHC Higgs data, we examine the parameter space of the type II two-Higgs-doublet model, in which the 125 GeV Higgs bosons exhibit wrong sign Yukawa couplings. Combining the relevant theoretical and experimental limits, we find that the LHC Higgs data exclude most of the parameter space of the wrong sign Yukawa coupling. For m_H = 600 GeV, the allowed samples are mainly distributed across several corners and narrow bands of m_A < 20 GeV, 30 < m_A < 120 GeV, 240 GeV < m_A < 300 GeV, 380 GeV < m_A < 430 GeV, and 480 GeV < m_A < 550 GeV. For m_A = 600 GeV, m_H is required to be lower than 470 GeV. The light pseudo-scalar with a mass of 20 GeV is still permitted in the case of the wrong sign Yukawa coupling of 125 GeV Higgs bosons.

Keywords: new physics model, Higgs boson, LHC, Higgs data

DOI: 10.1088/1674-1137/44/7/073101

1 Introduction

The two-Higgs-doublet model (2HDM) [1] is a popular extension of the SM that introduces another $SU(2)_L$ Higgs doublet, which contains neutral *CP*-even Higgs bosons h and H, a neutral pseudoscalar A, and charged Higgs $H^{\pm}$. Four typical 2HDMs have absent flavor changing neutral currents at the tree level, namely type-I [2, 3], type II [2, 4], lepton-specific models, and flipped models [5–8]. In the type II model, the Yukawa couplings of leptons and down-type quarks can be enhanced by a factor $\tan\beta$. Therefore, the flavor observables and the LHC search for Higgs places stricter restrictions to the type II model than to the other three models. In the type II 2HDM, the 125 GeV Higgs can have a wrong sign Yukawa coupling besides an SM-like coupling. In comparison with the SM, at least one of the Yukawa couplings of the 125 GeV Higgs has an opposite sign in the couplings of gauge bosons, which was extensively studied in Refs. [9–24].

In beginning of 2017, we used the LHC Higgs data available at that time to explore the parameter space of type II 2HDM, and found that the $H/A \to \tau^+\tau^-$ and $A \to hZ$ modes can place strong restrictions on the parameter space of the wrong sign Yukawa coupling [22]. Recently, Refs. [23, 24] examined the parameter space with degenerate heavy Higgs masses in the framework of this model. In this study, we re-examine the wrong sign Yukawa coupling in the type II 2HDM and extensively scan over the parameter space by considering recent ATLAS and CMS Higgs data.

Our paper is organized as follows. In Sec. 2, we briefly introduce the type II 2HDM. Detailed numerical calculations are implemented in Sec. 3. We display the allowed parameter space by considering relevant theoretical and experimental restrictions in Sec. 4. In Sec. 5, we provide our conclusions.

2 Type II two-Higgs-doublet model

The scalar potential with a softly broken discrete Z_2 symmetry is given by [25]

$$\begin{aligned} V =& m_{11}^2(\Phi_1^\dagger\Phi_1) + m_{22}^2(\Phi_2^\dagger\Phi_2) - \left[m_{12}^2(\Phi_1^\dagger\Phi_2 + \text{h.c.})\right] \\ &+ \frac{\lambda_1}{2}(\Phi_1^\dagger\Phi_1)^2 + \frac{\lambda_2}{2}(\Phi_2^\dagger\Phi_2)^2 + \lambda_3(\Phi_1^\dagger\Phi_1)(\Phi_2^\dagger\Phi_2) \\ &+ \lambda_4(\Phi_1^\dagger\Phi_2)(\Phi_2^\dagger\Phi_1) + \left[\frac{\lambda_5}{2}(\Phi_1^\dagger\Phi_2)^2 + \text{h.c.}\right]. \end{aligned} \quad (1)$$

Received 17 January 2020, Published online 9 May 2020

* Supported by the National Natural Science Foundation of China (11975013) and the Natural Science Foundation of Shandong province (ZR2017JL002, ZR2017MA004)

1) E-mail: xfhan@ytu.edu.cn

We focus on the *CP*-conserving case, where all λ_i and m_{12}^2 are real. The two complex Higgs doublets have the hypercharge $Y=1$:

$$\Phi_1=\begin{pmatrix}\phi_1^+\\ \frac{1}{\sqrt{2}}(v_1+\phi_1^0+ia_1)\end{pmatrix},$$
$$\Phi_2=\begin{pmatrix}\phi_2^+\\ \frac{1}{\sqrt{2}}(v_2+\phi_2^0+ia_2)\end{pmatrix}. \quad (2)$$

In the above formula, v_1 and v_2 are the electroweak vacuum expectation values (VEVs) with $v^2=v_1^2+v_2^2=(246\,\text{GeV})^2$ and $\tan\beta=v_2/v_1$. After breaking of the spontaneous electroweak symmetry, we obtain five physical Higgs particles, two neutral *CP*-even h and H, one neutral pseudoscalar A, and a pair of charged scalars $H^\pm$.

The Yukawa interactions are given as

$$-\mathcal{L}=Y_{u2}\,\overline{Q}_L\tilde{\Phi}_2\,u_R+Y_{d1}\,\overline{Q}_L\Phi_1\,d_R+Y_{\ell 1}\,\overline{L}_L\Phi_1\,e_R+\text{h.c.}, \quad (3)$$

where $Q_L^T=(u_L,d_L)$, $L_L^T=(\nu_L,l_L)$, and $\widetilde{\Phi}_{1,2}=i\tau_2\Phi_{1,2}^*$. Y_{u2}, Y_{d1} and $Y_{\ell 1}$ are 3×3 matrices.

The neutral Higgs Yukawa couplings normalized to the SM are as follows.

$$\begin{aligned}&y_h^{f_i}=\left[\sin(\beta-\alpha)+\cos(\beta-\alpha)\kappa_f\right],\\ &y_H^{f_i}=\left[\cos(\beta-\alpha)-\sin(\beta-\alpha)\kappa_f\right],\\ &y_A^{f_i}=-i\kappa_f\ (\text{for u}),\quad y_A^{f_i}=i\kappa_f\ (\text{for d},\ \ell),\\ &\text{with}\ \kappa_d=\kappa_\ell\equiv-\tan\beta,\quad \kappa_u\equiv 1/\tan\beta. \end{aligned} \quad (4)$$

The Yukawa interactions of the charged Higgs are given as,

$$\mathcal{L}_Y=-\frac{\sqrt{2}}{v}H^+\left\{\bar{u}_i\left[\kappa_d(V_{\text{CKM}})_{ij}\,m_{dj}P_R-\kappa_u m_{ui}\,(V_{\text{CKM}})_{ij}\,P_L\right]d_j+\kappa_\ell\,\bar{\nu}m_\ell P_R\ell\right\}+\text{h.c.}, \quad (5)$$

where $i,j=1,2,3$.

The neutral Higgs couplings with gauge bosons normalized to the SM are

$$y_h^V=\sin(\beta-\alpha),\quad y_H^V=\cos(\beta-\alpha), \quad (6)$$

with V denoting W or Z.

In type II 2HDM, the SM-like Higgs has not only the SM-like coupling, but also the wrong sign Yukawa coupling,

$$\begin{aligned}&y_h^{f_i}\times y_h^V>0\ \text{for SM}-\text{like coupling},\\ &y_h^{f_i}\times y_h^V<0\ \text{for wrong sign Yukawa coupling}.\end{aligned} \quad (7)$$

In case of the SM-like coupling, the 125 GeV Higgs couplings are very close to those in the SM, which has an alignment limit. Here, we introduce the wrong sign Yukawa coupling. The absolute values of $y_h^{f_i}$ and y_h^V should be close to 1.0 because of the restrictions in 125 GeV Higgs signal data. Hence, we obtain

$$\begin{aligned}&y_h^{f_i}=-1+\epsilon,\ y_h^V\simeq 1-0.5\cos^2(\beta-\alpha)\ \text{for}\\ &\sin(\beta-\alpha)>0\ \text{and}\ \cos(\beta-\alpha)>0,\\ &y_h^{f_i}=1-\epsilon,\ y_h^V\simeq -1+0.5\cos^2(\beta-\alpha)\ \text{for}\\ &\sin(\beta-\alpha)<0\ \text{and}\ \cos(\beta-\alpha)>0.\end{aligned} \quad (8)$$

Here, $|\epsilon|$ and $|\cos(\beta-\alpha)|$ are significantly less than 1. From Eq. (4), we can obtain

$$\begin{aligned}&\kappa_f=\frac{-2+\varepsilon+0.5\cos(\beta-\alpha)^2}{\cos(\beta-\alpha)}<<-1\ \text{for}\\ &\sin(\beta-\alpha)>0\ \text{and}\ \cos(\beta-\alpha)>0,\\ &\kappa_f=\frac{2-\varepsilon-0.5\cos(\beta-\alpha)^2}{\cos(\beta-\alpha)}>>1\ \text{for}\\ &\sin(\beta-\alpha)<0\ \text{and}\ \cos(\beta-\alpha)>0.\end{aligned} \quad (9)$$

In type II 2HDM, the constraints of the B-meson and R_b require $\tan\beta$ to be greater than 1, which leads to $\kappa_d<-1$, $\kappa_\ell<-1$, and $0<\kappa_u<1$. Therefore, there is no wrong sign Yukawa coupling for the up-type quark. The wrong sign Yukawa couplings of the down-type quark and lepton for $\sin(\beta-\alpha)>0$ and $\cos(\beta-\alpha)>0$ may exist. Because of the factor "–2" in the numerator in Eq. (9), $\cos(\beta-\alpha)$ and $\tan\beta$ in the wrong sign Yukawa coupling region are greater than those in the SM-like coupling region.

3 Numerical calculations

We choose the light *CP*-even Higgs boson h as the SM-like Higgs with the mass of 125 GeV. The branching ratio of $b\to s\gamma$ places stringent restrictions on the charged Higgs mass of the type II 2HDM, which requires $m_{H^\pm}>570$ GeV [26].

In the calculation, we take account the following constraints and observables:

(1) The electroweak precision data and theoretical constraints: We use the 2HDMC [27] to consider the theoretical constraints from the vacuum stability, unitarity and perturbativity, and calculate the oblique parameters (S, T, U). We take the recent fit results for S, T, U in Ref. [28],

$$S=0.02\pm0.10,\ T=0.07\pm0.12,\ U=0.00\pm0.09, \quad (10)$$

with correlation coefficients,

$$\rho_{ST}=0.89,\ \rho_{SU}=0.54,\ \rho_{TU}=0.83. \quad (11)$$

(2) The heavy-flavor observables and R_b constraints: We use SuperIso-3.4 [29] to calculate the branching ratio of $B\to X_s\gamma$. Δm_{B_s} is calculated following the formulas of Ref. [30]. Furthermore, we consider the R_b constraints of bottom quarks in Z decays, which are calculated following the formulas of Refs. [31, 32]. Recently, the R_b observable was also considered in some studies on the 2HDM [33, 34]

(3) The 125 GeV Higgs signal data: We use the version 2.0 of Lilith [35] to perform the calculation of χ^2 for

the 125 GeV Higgs signal data combining the LHC run-I and run-II data (up to datasets of 36fb^{-1}). We are particularly concerned with the surviving samples for $\chi^2-\chi^2_{\rm min}\leqslant 6.18$, where $\chi^2_{\rm min}$ is the minimum of χ^2. These samples are within the 2σ range in the two-dimensional plane of model parameters.

(4) The LHC search for additional Higgs bosons: We use the HiggsBounds-4.3.1 [36, 37] to perform the exclusion limits from the Higgs search at LEP at 95% confidence level.

At the LHC run-I and run-II, the ATLAS and CMS searched the additional Higgs via its decay into various SM modes and some exotic channels. Because of the destructive interference contributions to $gg\to A$ production, which arise from the top-quark loop and the bottom-quark loop in the type II 2HDM, the cross-section decreases with the increasing $\tan\beta$, and reaches a minimum value for a moderate $\tan\beta$, which is dominated by the bottom-quark loop for a large enough value of $\tan\beta$. The cross-section of $gg\to H$ production not only depends on $\tan\beta$ and m_H, but also $\sin(\beta-\alpha)$. We calculate the cross-sections for A and H in the gluon fusion and $b\bar{b}$-associated production at NNLO in QCD via SusHi [38]. The cross-sections of H via the vector boson fusion process are derived from the data of the LHC Higgs Cross Section Working Group [39]. We use the 2HDMC to calculate the branching ratios of various decay channels of A and H. In Table 1 and Table 2, we show a complete list of the additional Higgs searches considered in this study. When $1\leqslant\tan\beta\leqslant 30$, the heavy charged scalar searches at LHC cannot impose restrictions on the model for $m_{H^\pm}>500$ GeV [40]. Thus, we do not include the heavy charged Higgs search.

For the $A\to hZ$ channel, the CMS collaboration presented the result of $h\to\tau^+\tau^-$ at the 13 TeV LHC with an integrated luminosity of 35.9 fb^{-1} in Ref. [78].

Table 1. Upper bounds on production cross-section times branching ratio of $\tau^+\tau^-$, $\mu^+\mu^-$, $\gamma\gamma$, WW, and ZZ for H and A searches at 95% C.L..

Channel	Experiment/TeV	Mass range/GeV	Luminosity/fb^{-1}
$gg/b\bar{b}\to H/A\to\tau^+\tau^-$	ATLAS 8 [41]	90-1000	19.5-20.3
$gg/b\bar{b}\to H/A\to\tau^+\tau^-$	CMS 8 [42]	90-1000	19.7
$gg/b\bar{b}\to H/A\to\tau^+\tau^-$	ATLAS 13 [43]	200-1200	13.3
$gg/b\bar{b}\to H/A\to\tau^+\tau^-$	CMS 13 [44]	90-3200	12.9
$gg\to H/A\to\tau^+\tau^-$	CMS 13 [45]	200-2250	36.1
$b\bar{b}\to H/A\to\tau^+\tau^-$	CMS 13 [45]	200-2250	36.1
$b\bar{b}\to H/A\to\tau^+\tau^-$	CMS 8 [46]	25-80	19.7
$b\bar{b}\to H/A\to\mu^+\mu^-$	CMS 8 [47]	25-60	19.7
$pp\to H/A\to\gamma\gamma$	ATLAS 13 [48]	200-2400	15.4
$gg\to H/A\to\gamma\gamma$	CMS 8+13 [49]	500-4000	12.9
$gg\to H/A\to\gamma\gamma+t\bar{t}H/A\,(H/A\to\gamma\gamma)$	CMS 8 [50]	80-110	19.7
$gg\to H/A\to\gamma\gamma+t\bar{t}H/A\,(H/A\to\gamma\gamma)$	CMS 13 [50]	70-110	35.9
$VV\to H\to\gamma\gamma+VH\,(H\to\gamma\gamma)$	CMS 8 [50]	80-110	19.7
$VV\to H\to\gamma\gamma+VH\,(H\to\gamma\gamma)$	CMS 13 [50]	70-110	35.9
$gg/VV\to H\to W^+W^-$	ATLAS 8 [51]	300-1500	20.3
$gg/VV\to H\to W^+W^-\,(\ell\nu\ell\nu)$	ATLAS 13 [52]	300-3000	13.2
$gg\to H\to W^+W^-\,(\ell\nu qq)$	ATLAS 13 [53]	500-3000	13.2
$gg/VV\to H\to W^+W^-\,(\ell\nu qq)$	ATLAS 13 [54]	200-3000	36.1
$gg/VV\to H\to W^+W^-\,(e\nu\mu\nu)$	ATLAS 13 [55]	200-3000	36.1
$gg/VV\to H\to ZZ$	ATLAS 8 [56]	160-1000	20.3
$gg\to H\to ZZ(\ell\ell\nu\nu)$	ATLAS 13 [57]	300-1000	13.3
$gg\to H\to ZZ(\nu\nu qq)$	ATLAS 13 [58]	300-3000	13.2
$gg/VV\to H\to ZZ(\ell\ell qq)$	ATLAS 13 [58]	300-3000	13.2
$gg/VV\to H\to ZZ(\ell\ell\ell\ell)$	ATLAS 13 [59]	200-3000	14.8
$gg/VV\to H\to ZZ(\ell\ell\ell\ell+\ell\ell\nu\nu)$	ATLAS 13 [60]	200-2000	36.1
$gg/VV\to H\to ZZ(\nu\nu qq+\ell\ell qq)$	ATLAS 13 [61]	300-5000	36.1

Table 2. Upper bounds on production cross-section times branching ratio for channels of Higgs-pair and a Higgs production in association with Z at 95% C.L..

Channel	Experiment/TeV	Mass range/GeV	Luminosity /fb^{-1}
$gg \to H \to hh \to (\gamma\gamma)(b\bar{b})$	CMS 8 [62]	250-1100	19.7
$gg \to H \to hh \to (b\bar{b})(b\bar{b})$	CMS 8 [63]	270-1100	17.9
$gg \to H \to hh \to (b\bar{b})(\tau^+\tau^-)$	CMS 8 [64]	260-350	19.7
$gg \to H \to hh \to b\bar{b}b\bar{b}$	ATLAS 13 [65]	300-3000	13.3
$gg \to H \to hh \to b\bar{b}b\bar{b}$	CMS 13 [66]	750-3000	35.9
$gg \to H \to hh \to (b\bar{b})(\tau^+\tau^-)$	CMS 13 [67]	250-900	35.9
$pp \to H \to hh$	CMS 13 [68]	250-3000	35.9
$gg \to A \to hZ \to (\tau^+\tau^-)(\ell\ell)$	CMS 8 [64]	220-350	19.7
$gg \to A \to hZ \to (b\bar{b})(\ell\ell)$	CMS 8 [69]	225-600	19.7
$gg \to A \to hZ \to (\tau^+\tau^-)Z$	ATLAS 8 [70]	220-1000	20.3
$gg \to A \to hZ \to (b\bar{b})Z$	ATLAS 8 [70]	220-1000	20.3
$gg/b\bar{b} \to A \to hZ \to (b\bar{b})Z$	ATLAS 13 [71]	200-2000	36.1
$gg/b\bar{b} \to A \to hZ \to (b\bar{b})Z$	CMS 13 [72]	225-1000	35.9
$gg \to h \to AA \to \tau^+\tau^-\tau^+\tau^-$	ATLAS 8 [73]	4-50	20.3
$pp \to h \to AA \to \tau^+\tau^-\tau^+\tau^-$	CMS 8 [74]	5-15	19.7
$pp \to h \to AA \to (\mu^+\mu^-)(b\bar{b})$	CMS 8 [74]	25-62.5	19.7
$pp \to h \to AA \to (\mu^+\mu^-)(\tau^+\tau^-)$	CMS 8 [74]	15-62.5	19.7
$pp \to h \to AA \to (b\bar{b})(\tau^+\tau^-)$	CMS 13 [75]	15-60	35.9
$pp \to h \to AA \to \tau^+\tau^-\tau^+\tau^-$	CMS 13 [76]	4-15	35.9
$gg \to A(H) \to H(A)Z \to (b\bar{b})(\ell\ell)$	CMS 8 [77]	40-1000	19.8
$gg \to A(H) \to H(A)Z \to (\tau^+\tau^-)(\ell\ell)$	CMS 8 [77]	20-1000	19.8

However, compared to the results of Refs. [71, 72], the decay width Γ_A/m_A corresponding to the bound of Ref. [78] is not clearly given. Therefore, we do not include the experimental bound of $A \to hZ \to (\tau^+\tau^-)Z$ channel from Ref. [78].

4 Results and discussions

4.1 Constraints from oblique parameters and 125 GeV Higgs signal data

In Fig. 1, we display the permitted m_A and m_H under the constraints of theory and oblique parameters. Since the branching fraction of $b \to s\gamma$ imposes a lower bound on the mass of $H^\pm$, $m_{H^\pm} > 570$ GeV [26], we take 570 GeV $\leqslant m_{H^\pm} \leqslant$ 900 GeV. When either m_A or m_H are very close to $m_{H^\pm}$, the contributions of 2HDM to oblique parameters are considerably suppressed, and the other mass is permitted to have a large mass splitting with $m_{H^\pm}$. Therefore, as shown in Fig. 1, it is not feasible that both m_A and m_H are less than 480 GeV, and at least one of the A or H is required to have a greater mass. When either m_A or m_H is approximately 600 GeV, the other mass may have a large mass range, particularly for a low mass. However, when m_H is significantly larger than 600 GeV and even $m_H = m_{H^\pm}$, m_A cannot be very small. The main reason is due to the requirements of vacuum stability,

$$\lambda_1 > 0,\ \ \lambda_2 > 0,\ \ \lambda_3 > -\sqrt{\lambda_1\lambda_2},\ \ \lambda_3+\lambda_4-|\lambda_5| > -\sqrt{\lambda_1\lambda_2}. \tag{12}$$

To better understand this point, we assume a very small $\cos(\beta-\alpha)$ and obtain the following relations [18],

$$\begin{aligned}
v^2\lambda_1 &= m_h^2 - \frac{t_\beta(m_{12}^2 - m_H^2 s_\beta c_\beta)}{c_\beta^2},\\
v^2\lambda_2 &= m_h^2 - \frac{(m_{12}^2 - m_H^2 s_\beta c_\beta)}{t_\beta s_\beta^2},\\
v^2\lambda_3 &= m_h^2 + 2m_{H^\pm}^2 - 2m_H^2 - \frac{(m_{12}^2 - m_H^2 s_\beta c_\beta)}{s_\beta c_\beta},\\
v^2\lambda_4 &= m_A^2 - 2m_{H^\pm}^2 + m_H^2 + \frac{(m_{12}^2 - m_H^2 s_\beta c_\beta)}{s_\beta c_\beta},\\
v^2\lambda_5 &= m_H^2 - m_A^2 + \frac{(m_{12}^2 - m_H^2 s_\beta c_\beta)}{s_\beta c_\beta},
\end{aligned} \tag{13}$$

with $t_\beta \equiv \tan\beta$, $s_\beta \equiv \sin\beta$, and $c_\beta \equiv \cos\beta$. The first two requirements in Eq. (12) are simultaneously satisfied for $m_{12}^2 - m_H^2 s_\beta c_\beta \to 0$, and the last two are respectively satis-

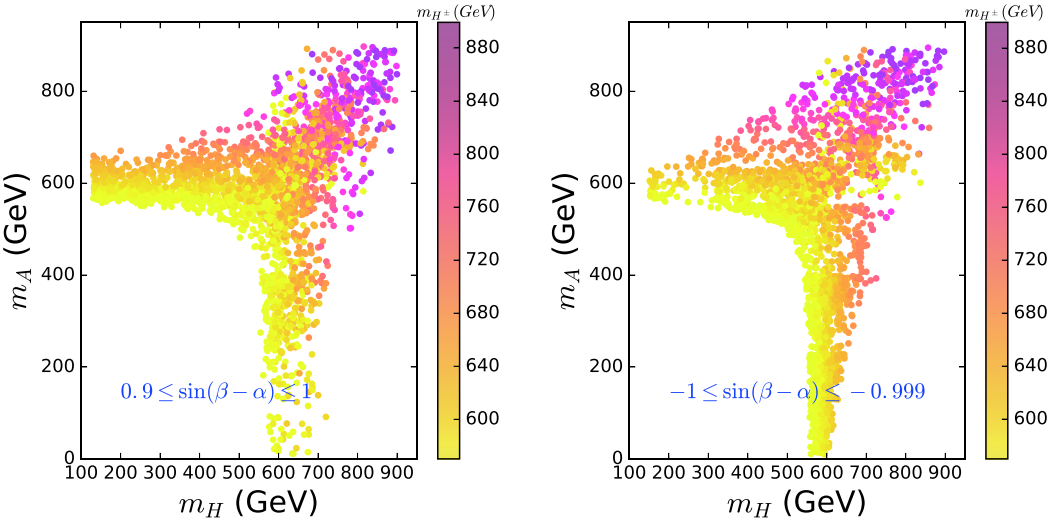

Fig. 1. (color online) Scatter plots of m_A and m_H satisfying constraints of vacuum stability, unitarity, perturbativity, and oblique parameters for $570 \leqslant m_{H^\pm} \leqslant 900$ GeV.

fied for

$$m_h^2 + m_{H^\pm}^2 - m_H^2 > 0, \qquad m_h^2 + m_A^2 - m_H^2 > 0. \tag{14}$$

The right relation of Eq. (14) implies that m_A cannot be very small for a very large m_H. Eq. (14) is obtained in the two limits, $\cos(\beta-\alpha) \to 0$ and $m_{12}^2 - m_H^2 s_\beta c_\beta \to 0$. In this study, we perform an exact numerical calculation on the requirements of vacuum stability. The bounds of Eq. (14) can be appropriately loosened by tunning $\cos(\beta-\alpha)$, t_β, and m_{12}^2.

Using the survival samples in Fig. 1 and imposing the restrictions of the 125 GeV Higgs signal data, we obtain the scatter plots of $\tan\beta$ and $\sin(\beta-\alpha)$ in Fig. 2. Fig. 2 shows that the 125 GeV Higgs data can provide very stringent constraints on $\tan\beta$ and $\sin(\beta-\alpha)$. As discussed above, the Yukawa coupling with the wrong sign can be achieved only for $\sin(\beta-\alpha) > 0$. In the left panel of Fig. 2, $\tan\beta$ and $\sin(\beta-\alpha)$ are respectively required to be larger than 5.0 and as low as 0.94 in case of wrong sign coupling. When the SM-like coupling is applied, $\sin(\beta-\alpha)$ is restricted to exist in two very narrow bands of $0.994 \sim 1.0$ and $-1.0 \sim -0.99993$, which can be seen in the left and right panels of Fig. 2. For a given $\sin(\beta-\alpha)$, $\tan\beta$ is imposed a lower limit in case of the Yukawa coupling with wrong sign, and it is required to be as low as 1.0 in case of the SM-like Higgs coupling.

To explicitly show the dependence of m_A (m_H) on the other parameters and the specific excluded parameter space from each channel, we do not simultaneously scan over m_A and m_H. In the following discussions, consider-

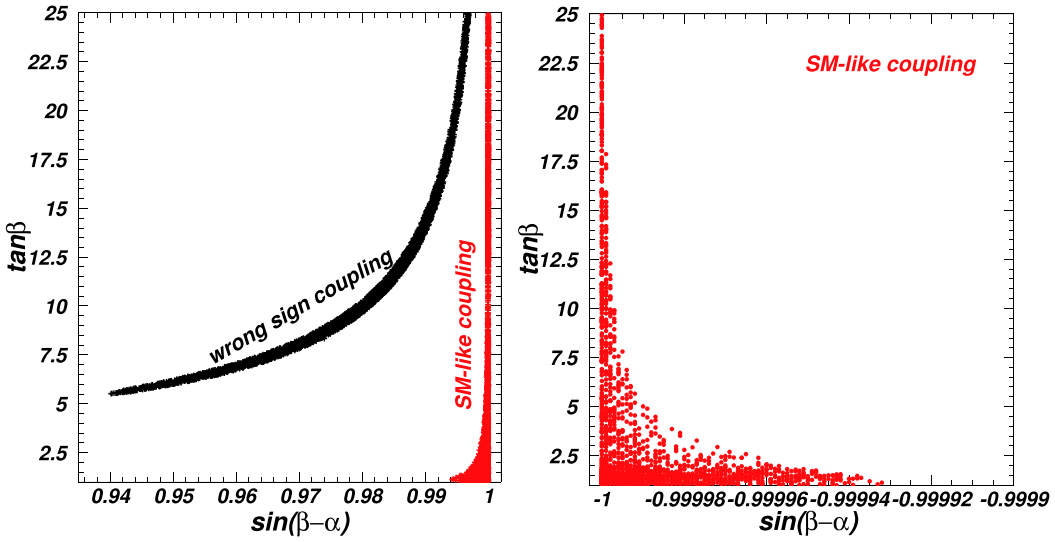

Fig. 2. (color online) Scatter plots of $\sin(\beta-\alpha)$ and $\tan\beta$ satisfying constraints of theory, oblique parameters, and 125 GeV Higgs signal data.

ing the allowed Higgs mass spectrum shown in Fig. 1, we will respectively set m_A or m_H as 600 GeV, and the other can have a wide mass range, especially for the low mass. Because heavy Higgs can easily avoid the restrictions of the LHC direct search easily, the Higgs with a moderate and low mass is more interesting. We scan the parameters for wrong sign Yukawa coupling in the following two scenarios:

$$\begin{aligned}&0.93 \leqslant \sin(\beta-\alpha) \leqslant 1.0,\ \ 1 \leqslant \tan\beta \leqslant 25,\\&570\ \text{GeV} \leqslant m_{H^\pm} \leqslant 900\ \text{GeV},\\&\text{scenario A}:\ \ m_H = 600\ \text{GeV},\ \ 10\ \text{GeV} \leqslant m_A \leqslant 900\ \text{GeV},\\&\text{scenario B}:\ \ m_A = 600\ \text{GeV},\ \ 150\ \text{GeV} \leqslant m_H \leqslant 900\ \text{GeV}.\end{aligned} \tag{15}$$

The free parameter m_{12}^2 is adjusted to satisfy the theoretical constraint. Here, we employ the conventional method [27], $0 \leqslant \beta \leqslant \frac{\pi}{2}$ and $-\frac{\pi}{2} \leqslant \beta-\alpha \leqslant \frac{\pi}{2}$. Namely, $0 \leqslant \cos(\beta-\alpha) \leqslant 1$ and $-1 \leqslant \sin(\beta-\alpha) \leqslant 1$.

4.2 Constraints on scenario A

We extract the permitted parameter space of scenario A after considering the joint constraints from pre-LHC (i.e., theoretical constraints, electroweak precision data, flavor observables, R_b, and exclusions from the search for Higgs at LEP), 125 GeV Higgs signal data, and the search for additional Higgs particles at the LHC. The surviving samples are projected on the planes of m_A versus $\tan\beta$ and m_A versus $\sin(\beta-\alpha)$ in Fig. 3. In case of the wrong sign Yukawa coupling, the restrictions mentioned above require $\tan\beta > 5$. For this range of $\tan\beta$, the cross-section of scalar A in the gluon fusion production is considerably suppressed, and all samples are favored by the $A \to \gamma\gamma$ and $A \to HZ$ modes. Because the 125 GeV Higgs signal data place large restrictions on the branching ratio of $h \to AA$, the LHC search for $h \to AA$ cannot impose constraints on the parameter space.

The $b\bar{b} \to A \to \tau^+\tau^-$ channel excludes most of the parameter space for large $\tan\beta$ and $gg/b\bar{b} \to A \to hZ$ for small $\tan\beta$. Because the coupling of AhZ is proportional to $\cos(\beta-\alpha)$, the $A \to hZ$ channel tends to exclude samples with small $|\sin(\beta-\alpha)|$. The permitted samples are mainly distributed across several corners and narrow bands. As shown in Table 1, the experimental bound of $A \to \tau^+\tau^-$ channel is absent for $m_A < 20$ GeV and $80 < m_A < 90$ GeV. Therefore, m_A in these mass ranges are permitted. Furthermore, most samples with m_A in the ranges of 30 ~ 120 GeV, 240 ~ 300 GeV, 380 ~ 430 GeV, and 480 ~ 550 GeV are allowed for appropriate $\tan\beta$ and $\sin(\beta-\alpha)$. For the last two bands, the experimental bounds of $A \to hZ$ [72] are larger than those of the neighbouring mass ranges. Therefore, in the regions of $380 \leqslant m_A \leqslant 430$ GeV and $480\ \text{GeV} \leqslant m_A \leqslant 550$ GeV, numerous samples with large $\sin(\beta-\alpha)$ can accommodate the bound of the $A \to hZ$ channel.

4.3 Constraints on scenario B

We study the permitted parameter space in scenario B when imposing the joint restrictions (1)–(4) in Section 3. The surviving samples are shown in the scatter plots of m_H with respect to $\tan\beta$ and $\sin(\beta-\alpha)$ in Fig. 4. Similar to the discussion in scenario A, the pre-LHC and 125 GeV Higgs signal data require $\tan\beta > 5$, and all samples are favored by the $H \to VV$, $\gamma\gamma$, hh, and $A \to HZ$ channels.

Fixing $m_A = 600$ GeV, the channel $b\bar{b} \to H \to \tau^+\tau^-$

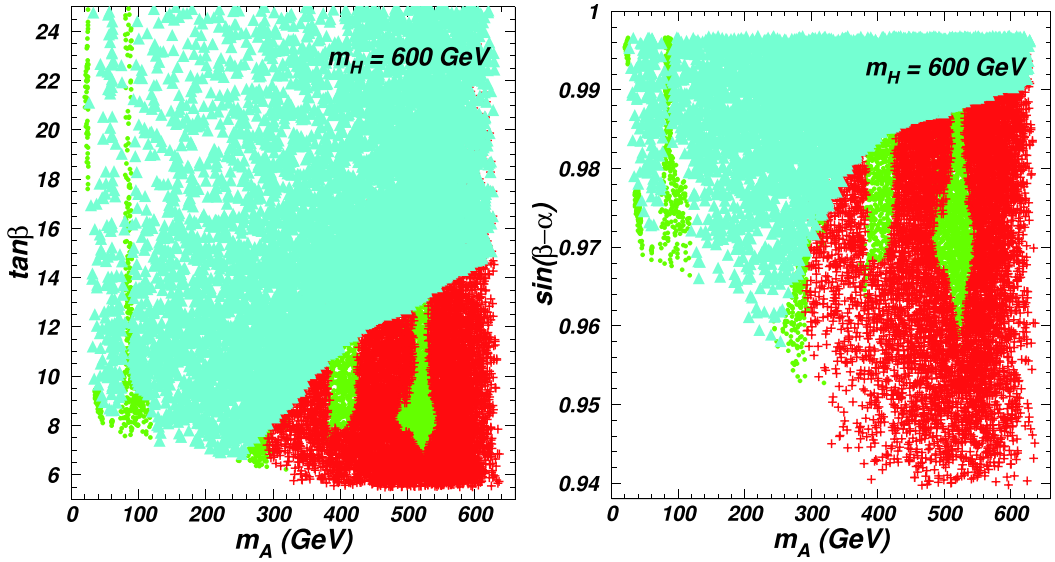

Fig. 3. (color online) Scatter plots of m_A with respect to $\tan\beta$ and m_A with respect to $\sin(\beta-\alpha)$ satifying constraints of pre-LHC and 125 GeV Higgs signal data. Triangles (sky blue) and pluses (red) are excluded by $A/H \to \tau^+\tau^-$ and $A \to hZ$ channels at the LHC, respectively. Bullets (green) are permitted by various LHC direct searches.

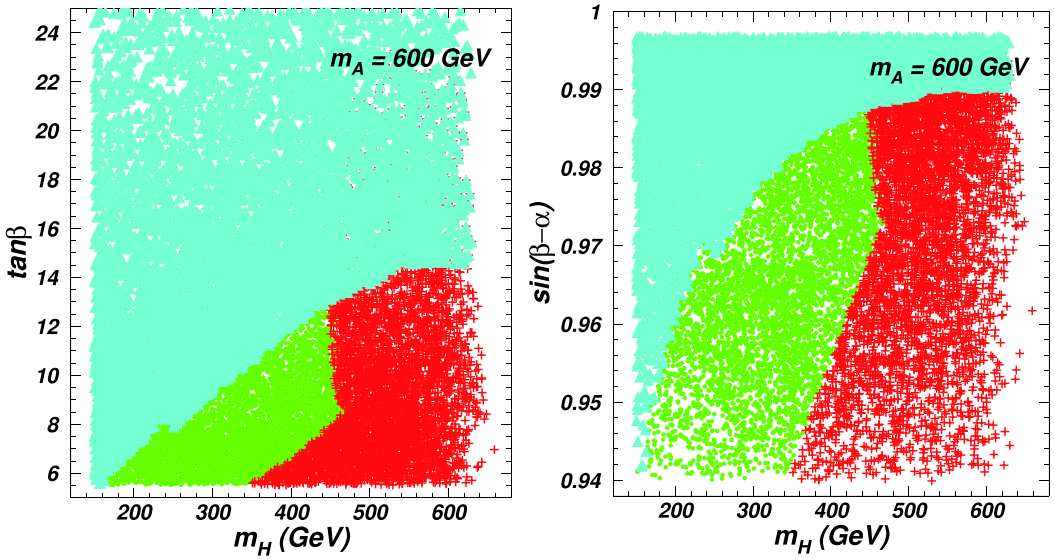

Fig. 4. (color online) Scatter plots of m_H with respect to tanβ and m_H versus sin$(\beta-\alpha)$ satisfying constraints of pre-LHC and 125 GeV Higgs signal data. Triangles (sky blue) and pluses (red) are excluded by $H/A \to \tau^+\tau^-$ and $A \to hZ$ channels at LHC, respectively. Bullets (green) are permitted by various LHC direct searches.

provides upper bounds on tanβ and sin$(\beta-\alpha)$. For instance, tan$\beta < 7.0$ (9.2, 14,4) and sin$(\beta-\alpha) < 0.96$ (0.98, 0.99) for $m_H =$ 200 GeV (300 GeV, 600 GeV). All samples with $m_H < 350$ GeV can accommodate the constraints from the channel $A \to hZ$. For such $m_H$values, the mode $A \to HZ$ can increase the total width of A and considerably suppress the branching ratio of $A \to hZ$. The channels $A \to \tau^+\tau^-$ and $A \to hZ$ exclude all samples with $m_H > 470$ GeV, and some samples with $150 < m_H < 470$ GeV survive for appropriate tanβ and sin$(\beta-\alpha)$.

In comparison with the results of Ref. [22], recent LHC Higgs data considerably reduce the parameter space. For $m_H = 600$ GeV, the whole range of $m_A < 700$ GeV is permitted in Ref. [22], while m_A is only allowed to vary within several ranges in this study, namely $m_A < 20$ GeV, $30 < m_A < 120$ GeV, 240 GeV $< m_A < 300$ GeV, 380 GeV $< m_A < 430$ GeV, and 480 GeV $< m_A < 550$ GeV. For $m_A = 600$ GeV, the entire range of $m_H < 700$ GeV is permitted in Ref. [22], while $m_H < 470$ GeV is required in this study. Such differences are mainly due to the experimental data of $gg/b\bar{b} \to A \to hZ$ from Refs. [71, 72], which are not included in Ref. [22].

5 Conclusion

We studied the status of wrong sign Yukawa coupling of type II 2HDM in light of recent LHC Higgs data, obtaining some interesting conclusions. The channels $b\bar{b} \to A/H \to \tau^+\tau^-$ and $gg/b\bar{b} \to A \to hZ$ exclude most of the parameter space for large tanβ and small tanβ, respectively. For $m_H =$ 600 GeV, the allowed samples are mainly distributed in several corners and narrow bands of $m_A < 20$ GeV, $30 < m_A < 120$ GeV, 240 GeV $< m_A < 300$ GeV, 380 GeV $< m_A < 430$ GeV, and 480 GeV $< m_A < 550$ GeV. For $m_A = 600$ GeV, m_H is required to be lower than 470 GeV.

References

1 T. D. Lee, Phys. Rev. D, **8**: 1226 (1973)
2 H. E. Haber, G. L. Kane, and T. Sterling, Nucl. Phys. B, **161**: 493 (1979)
3 L. J. Hall and M. B. Wise, Nucl. Phys. B, **187**: 397 (1981)
4 J. F. Donoghue and L. F. Li, Phys. Rev. D, **19**: 945 (1979)
5 V. D. Barger, J. L. Hewett, and R. J. N. Phillips, Phys. Rev. D, **41**: 3421 (1990)
6 Y. Grossman, Nucl. Phys. B, **426**: 3 (1994)
7 A. G. Akeroyd and W. J. Stirling, Nucl. Phys. B, **447**: 3 (1995)
8 A. G. Akeroyd, Phys. Lett. B, **377**: 95 (1996)
9 I. F. Ginzburg, M. Krawczyk, and P. Osland, arXiv: hep-ph/0101208
10 P. M. Ferreira, J. F. Gunion, H. E. Haber and R. Santos, Phys. Rev. D 89, 115003(2014).
11 B. Dumont, J. F. Gunion, Y. Jiang *et al*., Phys. Rev. D, **90**: 035021 (2014)
12 D. Fontes, J. C. Romo and J. P. Silva, Phys. Rev. D 90, 015021(2014).
13 P. M. Ferreira, J. F. Gunion, H. E. Haber *et al*., Phys. Rev. D, **89**: 115003 (2014)
14 D. Fontes, J. C. Romao, and J. P. Silva, Phys. Rev. D, **90**: 015021 (2014)
15 P. M. Ferreira, R. Guedes, M. O. P. Sampaio *et al*.., JHEP, **1412**: 067 (2014)
16 L. Wang and X.-F. Han, JHEP, **1505**: 039 (2015)
17 G. C. Dorsch, S. J. Huber, K. Mimasu *et al*., Phys. Rev. D, **93**:

115033 (2016)
18 F. Kling, J. M. No, and S. Su, JHEP, **1609**: 093 (2016)
19 A. Biswas and A. Lahiri, Phys. Rev. D, **93**: 115017 (2016)
20 T. Modak, J. C. Romao, S. Sadhukhan *et al*., Phys. Rev. D, **94**: 075017 (2016)
21 P. M. Ferreira, S. Liebler, and J. Wittbrodt, Phys. Rev. D, **97**: 055008 (2018)
22 L. Wang, F. Zhang, and X.-F. Han, Phys. Rev. D, **95**: 115014 (2017)
23 W. Su, M. White, A. G. Williams *et al*., arXiv: 1909.09035.
24 W. Su, arXiv: 1910.06269
25 R. A. Battye, G. D. Brawn, and A. Pilaftsis, JHEP, **1108**: 020 (2011)
26 Heavy Flavor Averaging Group, Eur. Phys. Jour. C, **77**: 895 (2017); M. Misiak and M. Steinhauser, Eur. Phys. Jour. C, **77**: 201 (2017)
27 D. Eriksson, J. Rathsman, and O. Stål, Comput. Phys. Commun., **181**: 189 (2010)
28 M. Tanabashi *et al*., Phys. Rev. D, **98**: 030001 (2018)
29 F. Mahmoudi, Comput. Phys. Commun., **180**: 1579-1673 (2009)
30 C. Q. Geng and J. N. Ng, Phys. Rev. D, **38**: 2857 (1988) [Erratum-ibid. D ,**41**: 1715 (1990)]
31 H. E. Haber and H. E. Logan, Phys. Rev. D, **62**: 015011 (2010)
32 G. Degrassi and P. Slavich, Phys. Rev. D, **81**: 075001 (2010)
33 N. Chen, J. Gu, T. Han *et al*., Int. J. Phys. A, **34**: 1940012 (2019)
34 N. Chen, T. Han, S. Li *et al*., arXiv: 1912.01431
35 J. Bernon, B. Dumont, and S. Kraml, Phys. Rev. D, **90**: 071301 (2014)
36 P. Bechtle, O. Brein, S. Heinemeyer *et al*., Comput. Phys. Commun., **181**: 138-167 (2010)
37 P. Bechtle, O. Brein, S. Heinemeyer *et al*., Eur. Phys. Jour. C, **74**: 2693 (2014)
38 R. V. Harlander, S. Liebler, and H. Mantler, Comput. Phys. Commun., **184**: 1605 (2013)
39 S. Heinemeyer *et al.* (LHC Higgs Cross Section Working Group Collaboration), arXiv: 1307.1347.
40 S. Moretti, arXiv: 1612.02063
41 G. Aad *et al*. (ATLAS Collaboration), JHEP, **11**: 056 (2014)
42 CMS Collaboration, CMS-PAS-HIG-14-029.
43 ATLAS Collaboration, ATLAS-CONF-2016-085
44 CMS Collaboration, CMS-PAS-HIG-16-037
45 ATLAS Collaboration, JHEP, **1801**: 055 (2018)
46 CMS Collaboration, Phys. Lett. B, **758**: 296-320 (2016)
47 CMS Collaboration, CMS-HIG-15-009
48 ATLAS Collaboration, ATLAS-CONF-2016-059
49 CMS Collaboration, CMS-PAS-EXO-16-027
50 CMS Collaboration, CMS-PAS-HIG-17-013
51 ATLAS Collaboration, G. Aad, *et al*., JHEP, **01**: 032 (2016)
52 ATLAS Collaboration, ATLAS-CONF-2016-074
53 ATLAS Collaboration, ATLAS-CONF-2016-062
54 ATLAS Collaboration, arXiv: 1710.07235
55 ATLAS Collaboration, Eur. Phys. Jour. C, **78**: 24 (2018)
56 ATLAS Collaboration, G. Aad, *et al*., Eur. Phys. Jour. C, **76**: 45 (2016)
57 ATLAS Collaboration, ATLAS-CONF-2016-056
58 ATLAS Collaboration, ATLAS-CONF-2016-082
59 ATLAS Collaboration, ATLAS-CONF-2016-079
60 ATLAS Collaboration, arXiv: 1712.06386
61 ATLAS Collaboration, arXiv: 1708.09638
62 V. Khachatryan *et al*. (CMS Collaboration), Phys. Rev. D, **94**: 052012 (2016)
63 V. Khachatryan *et al*. (CMS Collaboration), Phys. Lett. B, **749**: 560-582 (2015)
64 V. Khachatryan *et al*. (CMS Collaboration), Phys. Lett. B, **755**: 217-244 (2016)
65 ATLAS Collaboration, ATLAS-CONF-2016-049
66 CMS Collaboration, arXiv: 1710.04960
67 CMS Collaboration, arXiv: 1707.02909
68 CMS Collaboration, Phys. Rev. Lett., **122**: 121803 (2019)
69 V. Khachatryan *et al*. (CMS Collaboration), Phys. Lett. B, **748**: 221-243 (2015)
70 G. Aad *et al*. (ATLAS Collaboration), Phys. Lett. B, **744**: 163-183 (2015)
71 ATLAS Collaboration, arXiv: 1712.06518
72 CMS Collaboration, Eur. Phys. Jour. C, **79**: 564 (2019)
73 ATLAS Collaboration, Phys. Rev. D, **92**: 052002 (2015)
74 CMS Collaboration, JHEP, **1710**: 076 (2017)
75 CMS Collaboration, Phys. Lett. B, **785**: 462 (2018)
76 CMS Collaboration, arXiv: 1907.07235
77 V. Khachatryan *et al*. (CMS Collaboration), Phys. Lett. B, **759**: 369-394 (2016)
78 A. M. Sirunyan et al (CMS Collaboration), arXiv: 1910.11634